Journal of
Radiation Protection and Research 2024;49(2):85–90
https://doi.org/10.14407/jrpr.2024.00073

pISSN 2508-1888 | eISSN 2466-2461

Fabrication and Evaluation of Spectroscopic Grade Quasi-hemispherical CdZnTe Detector

Beomjun Park[1,2,3,*], Kyungeun Jung[4,*], Changsoo Kim[5]

[1]Department of Materials Science and Engineering, Korea University, Seoul, Korea; [2]The Institute for High Technology Materials and Devices, Korea University, Seoul, Korea; [3]Advanced Crystal Material/Device Research Center, Konkuk University, Seoul, Korea; [4]Agency for Defense Development (ADD), Daejeon, Korea; [5]Department of Radiological Science, College of Health Sciences, Catholic University of Pusan, Busan, Korea

ABSTRACT

Background: This study focuses on the fabrication and characterization of quasi-hemispherical $Cd_{0.9}Zn_{0.1}Te$ (CZT) detector for gamma-ray spectroscopy applications, aiming to contribute to advancements in radiation measurement and research.

Materials and Methods: A CZT ingot was grown using the vertical Bridgman technique, followed by proper fabrication processes including wafering, polishing, chemical etching, electrode deposition, and passivation. Response properties were evaluated under various external bias voltages using gamma-ray sources such as Co-57, Ba-133, and Cs-137.

Results and Discussion: The fabricated quasi-hemispherical CZT detector demonstrated sufficient response properties across a wide range of gamma-ray energies, with sufficient energy resolution and peak distinguishability. Higher external bias voltages led to improved performance in terms of energy resolution and peak shape. However, further improvements in defect properties are necessary to enhance detector performance under low bias conditions.

Conclusion: This study underscores the efficacy of quasi-hemispherical CZT detector for gamma-ray spectroscopy, providing valuable insights for enhancing their capabilities in radiation research field.

Keywords: CdZnTe, Spectroscopy, Quasi-hemispherical Detector, Gamma Ray, Semiconductor Detector

Technical Paper

Received March 22, 2024
Revision April 14, 2024
Accepted April 30, 2024

Corresponding author: Changsoo Kim

Department of Radiological Science, College of Health Sciences, Catholic University of Pusan, 57 Oryundae-ro, Geumjeong-gu, Busan 46252, Korea
E-mail: cszzim70@gmail.com
https://orcid.org/0000-0002-6380-0182

*These authors contributed equally to this work.

Introduction

Cadmium zinc telluride ($Cd_{0.9}Zn_{0.1}Te$ [CZT]) detectors have emerged as prominent figures in the field of room temperature semiconductor detectors (RTSD) [1, 2]. CZT (or RTSD) finds extensive applications across various domains, including nuclear medicine, medical physics, diagnostics, and nuclear detection [3–7]. Renowned for its strong stopping power, high effective atomic number, stability under high voltage, as well as sufficient transport properties and spectral performance, CZT has garnered significant attention [1]. Notably, the mobility-lifetime product of electrons and spectroscopy on 662 keV gamma ray (Cs-137) has reached around 10^{-1} cm^2/V and approximately 1% on its energy resolution, respectively [8–10]. Achieving such paramount performances necessitates a comprehensive consideration of moderate processes and external parameters such as fabrication techniques, electrode configurations, and external bias.

Spectroscopic-grade CZT crystals are typically grown utilizing melt-growing technol-

ogies such as the traveling heater method and the Bridgman technique [11, 12]. Throughout the CZT growth process, endeavors are made to maximize ingot volume and grain sizes while maintaining the homogeneous material properties of the ingot to ensure sufficient yield and the production of large-volume detectors. Correspondingly, the fabrication processes play a crucial role in transforming well-grown ingots into high-performance detectors.

In this study, we have designed quasi-hemispherical CZT detector employing a series of fabrication processes. Subsequently, we elucidated the effects of each fabrication step, the processing parameters, and gamma-ray spectroscopy of Cs-137 at different externally biased voltages. Furthermore, Co-57, Ba-133, and Cs-137 were introduced for spectroscopic characterization. The CZT demonstrated commendable performance in response properties, providing valuable guidance for RTSD fabrication and the interpretation of gamma-ray spectroscopy.

Materials and Methods

A CZT ingot with a diameter of approximately 5 cm was grown using the vertical Bridgman technique. The Bridgman furnace utilized in the process consisted of a single-zone heater with a temperature distribution set at moderate levels. For the synthesis of CZT, precursor materials included CdTe (6N), ZnTe (6N), Te (7N), and In for electrical compensation. The growth speed of CZT was maintained at 2.5 mm/hr. Upon completion of the growth phase, a lengthy cooling period of 72 hours was applied to mitigate stress and dislocation, which result from thermal expansion.

Subsequent to growth, wafering and dicing were performed using a wire saw, taking into account the grain boundary. Following this, mechanical polishing was conducted using Al_2O_3 powder ranging in size from 5 μm to 0.3 μm. Chemical etching with Br in MeOH was then applied, followed by deposition with a 5% $AuCl_3$ solution and passivation with NaClO [11].

The detector geometry was set to quasi-hemispherical configuration to ensure uniform charge collection and extraction for a single charge carrier (electron) [13]. The configuration enables superior performance on their energy resolution, by excluding the hole's contribution poorer in CdTe-based semiconductors [14].

Pulse height spectra of the detector were acquired by irradiating Co-57, Ba-133, and Cs-137 radioisotopes onto the cathode side of the detector, while signals were collected from a positively biased anode electrode. The utilized nuclear instruments included a CRZ-110 preamplifier (Cremat Inc.), CR-200 shaping amplifier (Cremat Inc.), Easy-MCA-8k (Amptek), and Ortec 659 (AMETEK Inc.) power supply. Customized sample holders were used to minimize the distance between the CZT and the preamplifier. Spectroscopic properties were measured after passivation under various bias voltages to observe the effects of external voltages. All measurements were conducted at 25 °C to eliminate temperature-induced effects.

Results and Discussion

Fig. 1 illustrates the progression of specimens through various fabrication steps. In Fig. 1A, cut wafers are depicted, showcasing distinct twins, grains, and their boundaries [15]. Volume defects such as inclusions and dislocations tend to accumulate at both grain and twin boundaries [15, 16], posing challenges for device performance when crystals with such defects are utilized in detector fabrication. Consequently, CZT must be extracted from regions within single grain to ensure optimal device performance. Subsequently, the extracted specimens are cut into hexahedron dimensions to facilitate appropriate device configuration and electric field for charge collection generated by radiation, as depicted in Fig. 1B. During this process, mechanical damages and cracks may occur at the specimen edges, potentially impeding device configuration and performance.

To mitigate these macro defects, a lapping and polishing process are undertaken employing a polisher, SiC polishing pad, and suitable abrasives like alumina (Al_2O_3). This process not only enhances electrical and surface quality of crystalline by eliminating rough surface imperfections but also ensures finer surface processing [17]. Following polishing with fine abrasives down to 1 μm or 0.3 μm, the surface achieves sufficient smoothness for camera photography as shown in Fig. 1C. Herein, the used camera was reflected by the smooth surface of CZT crystal, indicating very small roughness.

Mechanically processed specimens undergo chemical etching using a Br in MeOH solution, as depicted in Fig. 1D. This step aims to further smoothen crystal surfaces and eliminate micro-sized defects induced by mechanical fabrication, albeit at the expense of surface stoichiometry. Any non-stoichiometry induced by chemical etching is later compensated for during passivation after deposition. The smoother surface resulting from this process facilitates elec-

https://doi.org/10.14407/jrpr.2024.00073

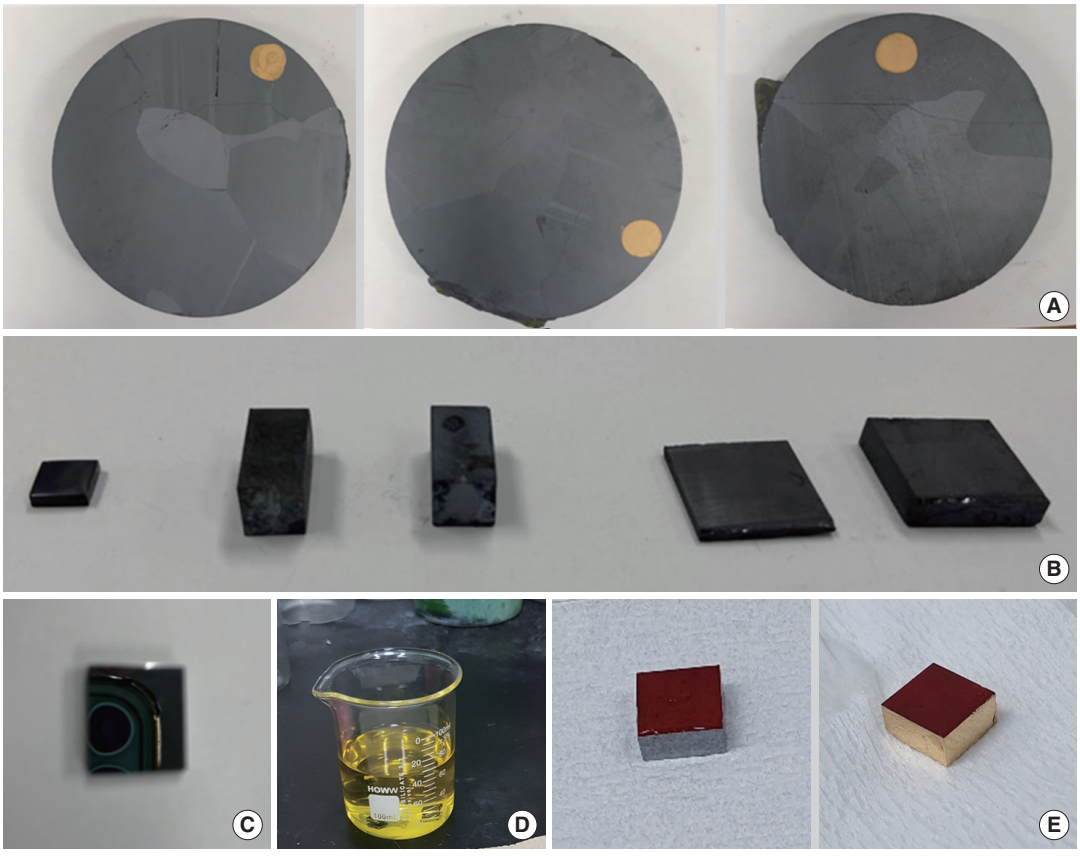

Fig. 1. Photographs of specimens at each step in a series of fabrication processes such as (A) wafering, (B) dicing, (C) lapping/polishing, (D) chemical etching, and (E) deposition. Specific device configuration is in Supplementary Fig. S1.

trode deposition on the crystal surface, ensuring homogeneous electric field distribution [18].

Fig. 1E showcases photographs of masking and electroless deposition to form the quasi-hemispherical configuration as illustrated in Supplementary Fig. S1. The quasi-hemispherical detector in this study was achieved through iterative processes including re-polishing, re-etching, re-depositing, and re-passivating the crystal as utilized in Park et al. [11]. Furthermore, the electrical and transport properties measured with quasi-hemispherical CZT configuration cannot directly represent the material's properties. Thus, the entire material properties such as resistance and mobility-lifetime product are confirmable with Park et al. [11], containing the measurements with planar- or bar-type CZT crystals grown under the same conditions as this study.

Fig. 2 depicts the response properties of the quasi-hemispherical CZT detector to 662 keV gamma rays emitted from Cs-137 radioisotopes under various external voltages. In Fig. 2A, the spectral results demonstrate the ability to distinguish the photopeak of 662 keV irrespective of voltages exceeding 500 V, corresponding to an electric field of 833 V/cm. The energy resolutions ranged from 10.5% to 4.5% with biases ranging from 500 V to 1,400 V, allowing for clear differentiation of the photopeak of 662 keV gamma rays. Higher external voltages exhibit improved performance in energy resolution and clearer shapes of photo- and backscatter-peaks. Broadening of peaks in the energy spectrum of semiconductor detectors originates from "incomplete charge," distinct from the originally generated charge amount by radiation. This incomplete charge arises from charge losses due to carrier recombination and trapping, influenced by semiconductor defects. Nevertheless, higher voltage facilitates faster carrier velocity (μE), enabling carriers to reach each collecting electrode swiftly and reducing exposure time on trapping centers [19–21].

Consequently, enhancements in bias voltage led to increases in peak centroid, peak height, peak-to-valley (P/V) ratio, and a decrease in valley count (Fig. 3 and Supplementary Table S1). These effects are discernible through over lapped spectra plots under various voltages, as illustrated in Fig. 2B, Supplementary Figs. S2 and S3. The photopeaks at

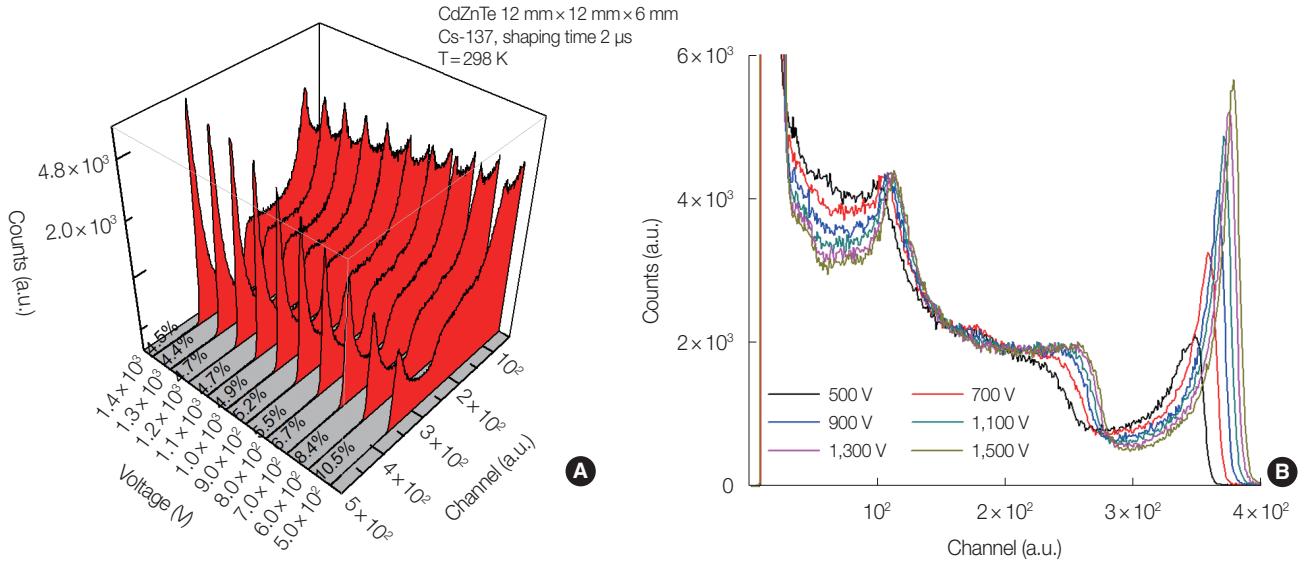

Fig. 2. Spectroscopic properties of quasi-hemispherical $Cd_{0.9}Zn_{0.1}Te$ (CZT) detector depending on the externally biased voltages obtained with Cs-137 radioisotope: (A) three dimensional plot (B) overlapped plot extracted from Supplementary Fig. S2 for clarifying. The different Y-axis scale of Fig. 2B shows 32 keV gamma rays as shown in Supplementary Fig. S3. The physical dimension for the detector is 12 mm × 12 mm × 6 mm. a.u., arbitrary unit.

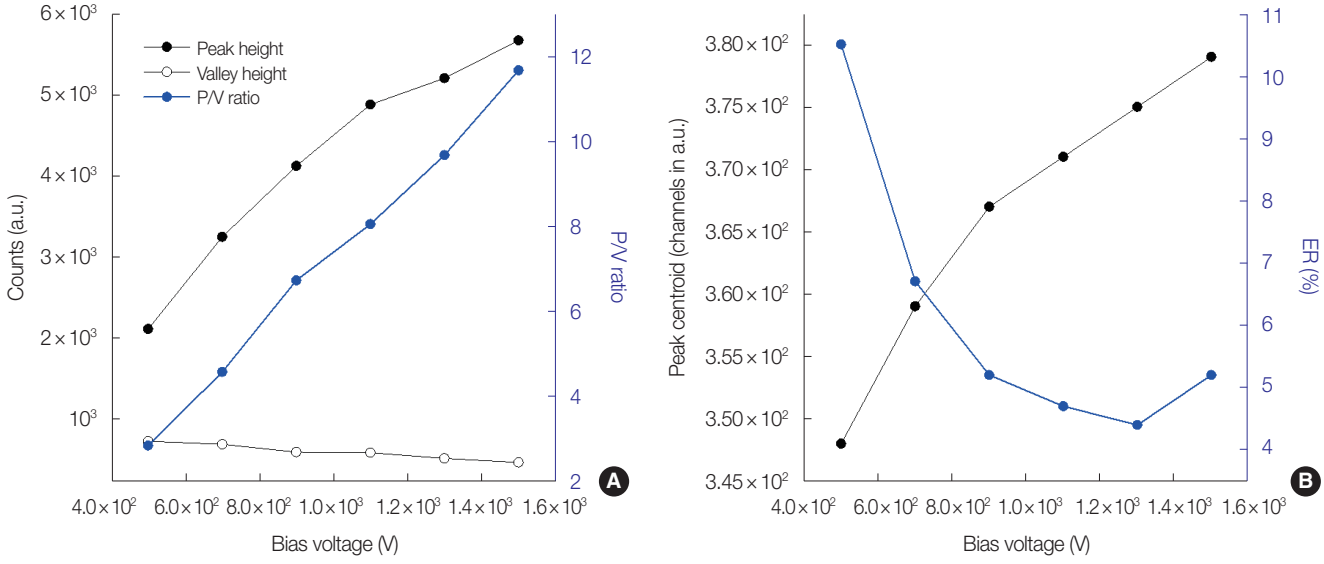

Fig. 3. Quantitative performances, including (A) the count and ratio of peaks/valleys, and (B) the peak centroid and energy resolution (ER), as a function of bias voltage. Specific values are presented in Supplementary Table S1. a.u., arbitrary unit; P/V, peak-to-valley.

channels ranging from 350 to 380 exhibit shifts with increasing bias due to the aforementioned reason, resulting in sharper peak shapes as the tails at low bias voltages re-stack onto the peak centroid. This phenomenon correlates with increases in P/V ratio, energy resolution, and peak height as shown in Fig. 3. Similar effects are observed in the Compton edge and backscattering peak, respectively located at channels 120 and 260. While the backscattering peak initially resembles an edge at 500 V, it becomes distinguishable with higher voltages. The Compton edge also becomes clearer with increased voltages. The final energy resolution on 662 keV emitted from Cs-137 radioisotope measures at 4.4%, comparable to commercial CZT detectors.

Fig. 4 illustrates the response properties of the quasi-hemispherical CZT detector to various gamma-ray sources; the gamma-ray energies span from 32 keV (Cs-137), 81 keV (Ba-133), 122 keV (Co-57), 303 keV (Ba-133), 356 keV (Ba-133) to 662 keV (Cs-137).

https://doi.org/10.14407/jrpr.2024.00073

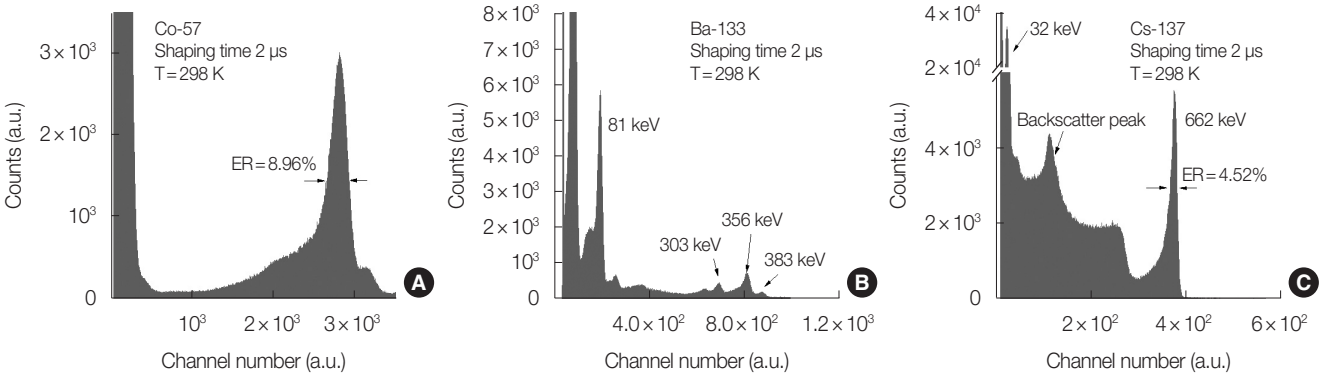

Fig. 4. Spectroscopic properties of quasi-hemispherical $Cd_{0.9}Zn_{0.1}Te$ (CZT) detector obtained with various radioisotopes: (A) Co-57, (B) Ba-133, and (C) Cs-137. External voltage was 1,400 V, which corresponds to 2,333 V/cm. a.u., arbitrary unit; ER, energy resolution.

In Fig. 4A, the pulse height spectrum from the Co-57 radioisotope emitting 122 keV and 136 keV gamma rays is presented. A notable energy resolution of 8.96% at 122 keV gamma rays is achieved, and the peak of 136 keV gamma rays is also distinguishable. This property is particularly significant as common planar CZT detectors often struggle to differentiate the gamma-peak of 136 keV [22].

Fig. 4B displays the resultant spectrum from the Ba-133 radioisotope, revealing photopeaks at energies of 81, 303, 356, and 383 keV. All peaks of Ba-133 are distinctly obtained with the quasi-hemispherical CZT detector, demonstrating its capability across a wide range of gamma-ray energies.

Fig. 4C showcases the response property of the CZT detector with the Cs-137 radioisotope emitting gamma rays at energies of 32 keV and 662 keV. Both peaks appear in the spectrum with sharp shapes, consistent with the explanation written in Fig. 2.

Overall, the response properties to gamma-rays spanning a wide energy range from 32 keV to 662 keV demonstrate sufficient energy resolution, indicating the efficacy of the quasi-hemispherical CZT detector in gamma-ray detection. However, there is room for improvement in defect properties such as dangling bonds, inner native defects, and Te inclusions, particularly considering the high electric field (2,333 V/cm) applied to maintain detector performance [16, 21, 23–25]. The high transport property, determined by crystal defect properties, is crucial for ensuring adequate performance under relatively lower bias conditions [21].

Conclusion

This study demonstrates the successful fabrication and characterization of a quasi-hemispherical CZT detector for gamma-ray spectroscopy applications. Through a series of fabrication processes and varying external bias voltages, the detector exhibited paramount response properties across a wide range of gamma-ray energies, with sufficient energy resolution and peak distinguishability. Despite the notable performance, further improvements in defect properties are warranted to maintain high detector performance under relatively low bias conditions. Overall, the findings underscore the efficacy of the quasi-hemispherical CZT detector and provide valuable guidance for enhancing its capabilities in gamma-ray detection and spectroscopy applications utilizing RTSD.

Supplementary Materials

Supplementary materials can be found via https://doi.org/10.14407/jrpr.2024.00073.

Conflict of Interest

No potential conflict of interest relevant to this article was reported.

Acknowledgements

Changsoo Kim was supported by a research grant in 2023 from the Catholic University of Pusan (CUP No. 2023-01-020).

Ethical Statement

This article does not contain any studies with human participants or animals performed by any of the authors.

Author Contribution

Conceptualization: Park B, Kim C. Methodology: Park B, Jung K. Formal analysis: Park B, Jung K. Funding acquisition: Kim C. Visualization: Park B, Jung K. Writing - original draft: Park B, Jung K. Writing - review & editing: Kim C. Approval of final manuscript: all authors.

References

1. Sordo SD, Abbene L, Caroli E, Mancini AM, Zappettini A, Ubertini P. Progress in the development of CdTe and CdZnTe semiconductor radiation detectors for astrophysical and medical applications. Sensors (Basel). 2009;9(5):3491–3526.
2. Takahashi T, Watanabe S. Recent progress in CdTe and CdZnTe detectors. IEEE Trans Nucl Sci. 2001;48(4):950–959.
3. Gregoire B, Pina-Jomir G, Bani-Sadr A, Moreau-Triby C, Janier M, Scheiber C. Four-minute bone SPECT using large-field cadmium-zinc-telluride camera. Clin Nucl Med. 2018;43(6):389–395.
4. Ergun J, Buchholz M, Payne RK, Gorsuch D, Bisek J, Ergun DL, et al. CZT detector for dual-energy X-ray absorptiometry (DEXA). Proceedings of SPIE 4142, Penetrating Radiation Systems and Applications II; 2000 Dec 18; San Diego, CA. Available from: https://doi.org/10.1117/12.410561
5. Fatemi S, Gong CH, Bortolussi S, Magni C, Postuma I, Bettelli M, et al. Innovative 3D sensitive CdZnTe solid state detector for dose monitoring in Boron Neutron Capture Therapy (BNCT). Nucl Instrum Methods Phys Res A. 2019;936:50–51.
6. Jo WJ, Jeong M, Kim HS, Kim SY, Ha JH. Preliminary research of CZT based PET system development in KAERI. J Radiat Prot Res. 2016;41(2):81–86.
7. Kim Y, Lee W. Development of a virtual Frisch-grid CZT detector based on the array structure. J Radiat Prot Res. 2020;45(1):35–44.
8. Bolotnikov AE, Camarda GS, Chen E, Cui Y, Gul R, Dedic V, et al. Using the TOF method to measure the electron lifetime in long-drift CdZnTe detectors. Proceedings of SPIE 9968, Hard X-Ray, Gamma-Ray, and Neutron Detector Physics XVIII; 2016 Nov 2; San Diego, CA. Available from: https://doi.org/10.1117/12.2240091
9. Chen H, Li H, Reef MD, Sundaram AG, Eger J, Hugg JW, et al. Development of large-volume high-performance monolithic CZT radiation detector. Proceedings of SPIE 10762, Hard X-Ray, Gamma-Ray, and Neutron Detector Physics XX; 2018 Sep 13; San Diego, CA. Available from: https://doi.org/10.1117/12.2321244
10. Cui Y, Bolotnikov AE, Camarda G, Hossain A, Yang G, James RB. CZT virtual Frisch-grid detector: principles and applications. Proceedings of 2009 IEEE Long Island Systems, Applications and Technology Conference; 2009 May 1; Farmingdale, NY. Available from: https://doi.org/10.1109/LISAT.2009.5031559
11. Park B, Kim Y, Seo S, Byun J, Kim K. Passivation effect on large volume CdZnTe crystals. Nucl Eng Technol. 2022;54(12):4620–4624.
12. Roy UN, Burger A, James RB. Growth of CdZnTe crystals by the traveling heater method. J Cryst Growth. 2013;379:57–62.
13. Zanio K. Use of various device geometries to improve the performance of CdTe detectors. Rev Phys Appl. 1977;12(2):343–347.
14. He Z. Review of the Shockley-Ramo theorem and its application in semiconductor gamma-ray detectors. Nucl Instrum Methods Phys Res A. 2001;463(1–2):250–267.
15. Roy UN, Camarda GS, Cui Y, Gul R, Hossain A, Yang G, et al. Role of selenium addition to CdZnTe matrix for room-temperature radiation detector applications. Sci Rep. 2019;9(1):1620.
16. Hwang S, Yu H, Bolotnikov AE, James RB, Kim K. Anomalous Te inclusion size and distribution in CdZnTeSe. IEEE Trans Nucl Sci. 2019;66(11):2329–2332.
17. Brovko A, Adelberg A, Chernyak L, Gorfman S, Ruzin A. Impact of polishing on crystallinity and static performance of $Cd_{1-x}Zn_xTe$. Nucl Instrum Methods Phys Res A. 2020;984:164568.
18. Park B, Ko J, Byun J, Pandey S, Park B, Kim J, et al. Solution-grown $MAPbBr_3$ single crystals for self-powered detection of X-rays with high energies above one megaelectron volt. Nanomaterials (Basel). 2023;13(15):2157.
19. Eisen Y, Horovitz Y. Correction of incomplete charge collection in CdTe detectors. Nucl Instrum Methods Phys Res A. 1994;353(1–3):60–66.
20. Butcher J, Hamade M, Petryk M, Bolotnikov AE, Camarda GS, Cui Y, et al. Drift time variations in CdZnTe detectors measured with alpha particles and gamma rays: their correlation with detector response. IEEE Trans Nucl Sci. 2013;60(2):1189–1196.
21. Bolotnikov AE, Abdul-Jabbar NM, Babalola OS, Camarda GS, Cui Y, Hossain A, et al. Effects of Te inclusions on the performance of CdZnTe radiation detectors. IEEE Trans Nucl Sci. 2008;55(5):2757–2764.
22. Park B, Kim Y, Seo J, Byun J, Dedic V, Franc J, et al. Bandgap engineering of $Cd_{1-x}Zn_xTe_{1-y}Se_y$ ($0<x<0.27$, $0<y<0.026$). Nucl Instrum Methods Phys Res A. 2022;1036:166836.
23. Kim Y, Ko J, Byun J, Seo J, Park B. Passivation effect on $Cd_{0.95}Mn_{0.05}Te_{0.98}Se_{0.02}$ radiation detection performance. Appl Radiat Isot. 2023;200:110914.
24. Fochuk P, Grill R, Panchuk O. The nature of point defects in CdTe. J Electron Mater. 2006;35:1354–1359.
25. Turjanska L, Hoschl P, Belas E, Grill R, Franc J, Moravec P. Defect structure of CdZnTe. Nucl Instrum Methods Phys Res A. 2001;458(1–2):90–95.

 https://doi.org/10.14407/jrpr.2024.00073